

# DISTRIBUTION OF ACTION POTENTIAL DURATION AND T-WAVE MORPHOLOGY: A SIMULATION STUDY

Elena Ryzhii<sup>1</sup>, Maxim Ryzhii<sup>2</sup>, and Daming Wei<sup>3</sup>

**Abstract** — The results of a simulation study of the action potential duration (APD) distribution and T-wave morphology taking into account the midmyocardial cells (M-cells) concept are described. To investigate the effect of M-cells we present a computer model in which ion channel action potential formulations are incorporated into three-dimensional whole heart model. We implemented inhomogeneous continuous action potential duration distribution based on different distributions of maximal slow delayed rectifier current conductance. Using the proposed action potential distribution procedure midmural zeniths with longest action potential length were created as islands of model cells in the depth of thickest areas of ventricular tissue. Different spatial functions on layer indexes were simulated and their influences on electrocardiogram waveforms were analyzed. Changing parameters of ion channel model we varied duration of minimal and maximal action potential and investigated T-wave amplitude,  $Q-T_{peak}$  and QT intervals variations. The study demonstrated that the proposed APD distribution is reasonable and produces realistic electrocardiographic waveforms.

**Index Terms** — whole heart model, ion channels, M-cell, T-wave

## I. INTRODUCTION

Transmural heterogeneity of action potentials is considered to be an important factor for understanding electrical properties of the heart and arrhythmic mechanisms. Experimental studies on isolated ventricular cells have demonstrated that three functionally different cell types exhibit distinct electrophysiological profile. These cell types include endocardial cells, epicardial cells, and a subpopulation of M-cells [1, 2]. It was demonstrated by Antzilevich et al (see, for example, [3]) that M-cells with APD longer than those of endocardial and epicardial cells are located in midmyocardium of left ventricular anterior and lateral walls and septum.

Although recently M-cells became a debated issue, we assume the presence of M-cells in the ventricular midwall and include them in our present study. It has been shown that transmural voltage gradients during repolarization contribute importantly to the T-wave and correlations have been found between cellular events and the surface signal.

Limited number of experimental works was performed on studies of action potential (AP) transmural heterogeneity in human myocardium [4, 5]. The results provide only partial information from isolated regions of the myocardial tissue and do not represent the entire heart. Still it remains unclear how exactly three types of ventricular cells (epi-, endo and midmyocardial) are distributed throughout the heart tissue. In computer simulation studies many researchers use 2D and 3D ventricular slab structures [6, 7] where these cells are located as discrete layers in different proportions based on studies of Drouin *et al* [4]. One can assume that such layered structure should not be homogeneous with constant APD in each layer, because such arrangement leads to great differences in duration on the borders between the cell layers. In particular, this is related to the right ventricle free wall where the tissue layer is thinnest. The heterogeneous structure with smooth changes from short to long, and then from long to short APD across the myocardial walls can overcome the APD discontinuity.

Continuous variation of APD across the ventricular wall has been shown in the experimental works [8, 9], which noted the reduction of the in vitro difference in APD between M-cells and endocardial/epicardial cells to much smaller in vivo values due to the effect of electrotonic coupling. The hypothesis of the continuous APD distribution found some confirmation in 3D whole heart computer simulations [10-12].

We present the development of the three-dimensional heart model first proposed by Aoki *et al* [13] based on theoretical studies of the T-wave by Harumi *et al* [14]. The model was expanded to the whole heart by Wei *et al* [15-18] and allows simulating the body surface electrocardiograms (ECGs) based on anatomical and electrophysiological settings. The model was utilized in different simulation studies (see, for example, [19, 20]), and demonstrated its reliability and adequacy in most cases.

In this study we utilize the modified whole heart model incorporating updated realistic ion channel model for calculating electrical AP of ventricular myocytes. We propose and consider smooth heterogeneous ventricular APD distributions depending on thickness variation of different myocardial walls. The APD distributions are based on continuous assignment of slow delayed rectifier current values.

<sup>1</sup> Elena Ryzhii, Biomedical Information Technology Laboratory, University of Aizu, Aizu-Wakamatsu, 965-8580 Japan eryzhii(at)ieee.org

<sup>2</sup> Maxim Ryzhii, Computational Nanoelectronics Laboratory, University of Aizu, Aizu-Wakamatsu, 965-8580 Japan m-ryzhii(at)u-aizu.ac.jp

<sup>3</sup> Daming Wei, Biomedical Information Technology Laboratory, University of Aizu, Aizu-Wakamatsu, 965-8580 Japan

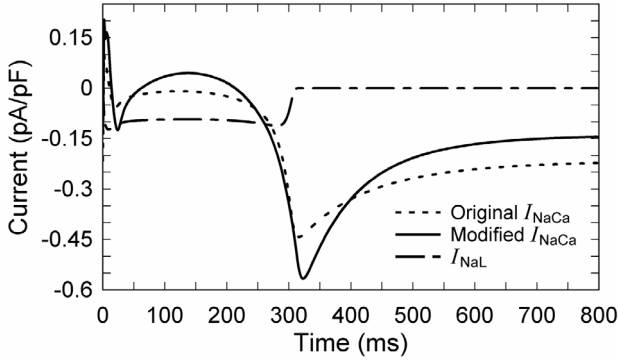


Figure 1. Calculated time dependencies of sodium-calcium exchanger current  $I_{NaCa}$  (for original and modified models) and late sodium current  $I_{NaL}$ .

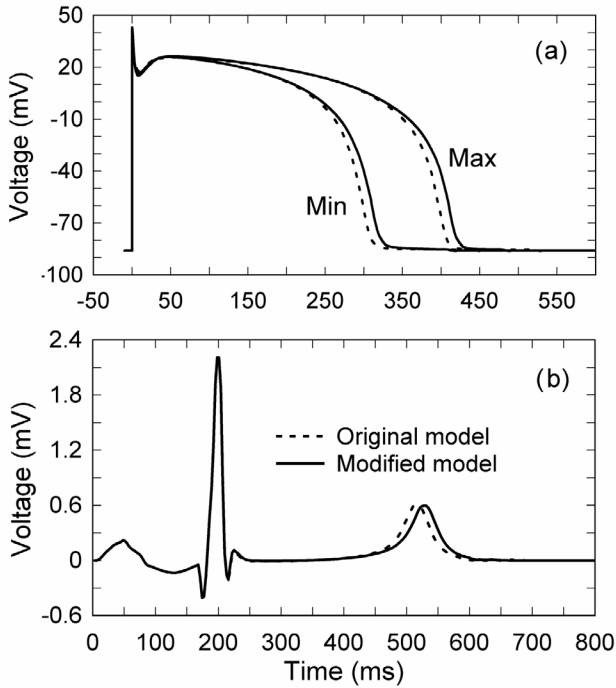


Figure 2. Comparison of original and modified ion channel models: (a) action potential waveforms with minimal (epicardial) and maximal (midmyocardial) durations and (b) lead V5 simulated ECG waveforms.

The purpose of this study is to analyze the validity of the proposed APD distribution of three myocardial cell types over the ventricular tissue, investigating the shape and amplitude of the T-wave, Q-T<sub>peak</sub> and QT intervals. Since the T-wave is the result of spatial heterogeneity in the ventricular APD, we vary the minimal and maximal APD of epicardial and midmyocardial cells and study its influence on the T-wave formation.

The paper is organized as follows. In Section II, we introduce the modifications in the ionic currents formulation of ion channel model and their impact on the AP and ECG waveform shapes. Details of the ion channel model are included in Appendix. Next, we briefly summarize the three-

dimensional whole heart model utilized in this study and propose an APD spatial distribution incorporating the M-cells. In Section III, we present simulated qualitative and quantitative results cardiac activity validating the proposed model. This is followed by discussion in Section IV and our conclusions in Section V.

## II. SIMULATION METHODS

### A. Ion Channel Model

In this study, we modified total transmembrane ionic current  $I_{ion}$  in the model of human ventricular myocytes of ten Tusscher and Panfilov [21] by changing formulation of sodium-calcium exchanger current  $I_{NaCa}$  and adding late (slowly inactivating) sodium current  $I_{NaL}$ . We fitted the parameters of ion channel kinetics to available experimental data from human ventricular myocytes to let our model APD lie more in the midrange of experimental data [22, 23]. General equations of the model and corresponding parameters for the currents are described in the Appendix.

Figure 1 shows the obtained time dependencies of  $I_{NaCa}$  for original and modified models and  $I_{NaL}$ . The calculated minimal (epicardial) and maximal (midmyocardial) AP and ECG waveforms for the modified model and its comparison with the original ten Tusscher model are demonstrated in the Fig. 2.

### B. Three-Dimensional Human Whole Heart Model

The 3D human whole-heart model consists of about 55,000 discrete units (model cells) representing atria and ventricles and mounted in homogeneous torso. The model is constructed in the close-packed cubic structure, and each unit is in direct contact with up to 12 adjacent, equidistant cells with 1.5 mm spatial resolution. These elements are arranged in matrix of 50x50x81 cells, each identified by three integers in a hexagonal coordinate system [15]. Cell-by-cell fiber direction is incorporated into the heart model by sorting the discrete cells into layers and setting the fiber orientation for each layer so as to have a total 90 degree fiber orientation gradually changed from the epicardium to the endocardium. The anisotropy in conduction velocity of propagation and electric conductivity is incorporated based on the fiber direction [16].

The propagation of excitation in the heart model is simulated based on the Huygens' Principle. At any time step, an ellipsoidal wavelet based on the local fiber direction is calculated. The long semiaxis of the wavelet along the fiber direction,  $R_l$ , and the other two short semiaxes along the two transversal directions,  $R_t$ , are determined with

$$R_l = V_l(t) \cdot T \quad (1)$$

and

$$R_t = R_l \cdot k_r \quad (2)$$

respectively, where  $T$  is the time step,  $V_l$  is the longitudinal conduction velocity of the cell at time  $t$ , and  $k_r$  is the conductivity ratio. The extent of wavelet propagation is described by

$$l^2/R_l^2 + n^2/R_t^2 + m^2/R_t^2 < 1, \quad (3)$$

where  $l$ ,  $n$ , and  $m$  are the distances along and across the fiber direction in the local coordinate system established at the exciting cell. Cells within the wavelet can be activated if they are excitable at that time, which is evaluated by refractory principle. The excitation of cardiac cells yields electrical current inside the heart as the electric cardiac source of the ECG.

The surface potentials on the model torso generated by the heart model were calculated by means of the boundary element method [24]. Surface potentials on all surface nodal points were calculated. The standard 12-lead ECG was calculated based on standard electrode positions.

The solution of the cardiac source is based on the spatial distribution of transmembrane potential resulted from the propagation of excitation. The modified Miller-Geselowitz formula was used taking into account the rotating anisotropic media [25]:

$$\vec{J} = -D_{in} \nabla \Phi_{in}, \quad (4)$$

where  $\vec{J}$  is the current dipole moment in the cardiac myocardium,  $D_{in}$  is the intracellular conductivity tensor, and  $\Phi_{in}$  is the intracellular potential.

For a homogeneous torso model, the following equation for potentials was used by applying Green's theorem to the torso surface:

$$\Phi(\vec{r}) = \frac{1}{4\pi\sigma} \int_v \vec{J} \cdot \nabla \left( \frac{1}{r} \right) dv + \frac{1}{4\pi} \int_s \Phi(\vec{r}) \nabla \left( \frac{1}{r} \right) ds, \quad (5)$$

where  $\Phi$  is the surface potential,  $\sigma$  is the conductivity, and  $r$  is a scale distance from  $dv(\vec{r})$  to  $ds(\vec{r})$ . The first term of this equation is equal to the potential which would be yielded in an infinite homogeneous medium owing to the cardiac source. The second term reflects the boundary effect. The Neumann's boundary condition is applied to the potential on torso surface, since the conductivity is zero outside the torso.

For the solutions of potential theory, the boundary element method was used. An intermediate variable  $\psi = \phi - \phi^0$  was introduced to reduce a Poisson equation with respect to  $\phi$ , to a Laplace equation with respect to  $\psi$ , with boundary condition of

$$\frac{\partial \psi}{\partial n} = \frac{\partial \phi^0}{\partial n} = -q^0. \quad (6)$$

where  $\phi$  and  $\phi^0$  are potentials in bounded and infinite media, respectively, and  $n$  represents normal direction to the body surface. Applying the boundary element method with respect to  $\psi$

$$\int_{sb} \psi \frac{\partial G}{\partial n} dS = - \int_{sb} q^0 G dS, \quad (7)$$

where  $G$  is the Green function of

$$G = \frac{1}{4\pi\vec{r} - \vec{r}'}, \quad (8)$$

where  $r$  is the distance from a dipole source and the integration is performed with respect to  $\vec{r}'$ . Discretization of the integral equation (7) leads to linear equations

$$\sum_{j=1}^N h_{ij} \phi_j = - \sum_{j=1}^N g_{ij} q_j^0 \quad i = 1, 2, \dots, N, \quad (9)$$

where  $h_{ij}$  and  $g_{ij}$  are coefficients depending on the torso geometry and  $N$  is the number of elemental triangles which approximates the torso surface. To ensure a unique solution for equation (9), an additional condition

$$\sum_{j=1}^N a_j \psi_j = - \sum_{j=1}^N a_j \phi_j^0 \quad (10)$$

is further imposed, where  $a_j$  is proportional to the area of an elemental triangle which has an apex  $j$ . This condition is used to define a potential reference so that the surface potential integral is zero. In matrix notation,

$$\mathbf{H}\Psi = -\mathbf{G}\mathbf{Q}^0 - \mathbf{A} \quad (11)$$

is obtained and the final solution for surface potentials is expressed as:

$$\Phi = \Phi^0 - \mathbf{M}\mathbf{Q}^0 - \mathbf{P}^0, \quad (12)$$

where

$$\mathbf{M} = (\mathbf{H}^T \mathbf{H})^{-1} \mathbf{H}^T \mathbf{G} \quad (13)$$

and

$$\mathbf{P}^0 = (\mathbf{H}^T \mathbf{H})^{-1} \mathbf{H}^T \mathbf{A}. \quad (14)$$

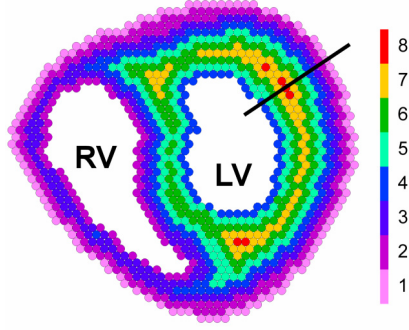


Figure 3. The horizontal cross-section of the heart model with sequence layers. RV and LV represent the right and left ventricles, respectively.

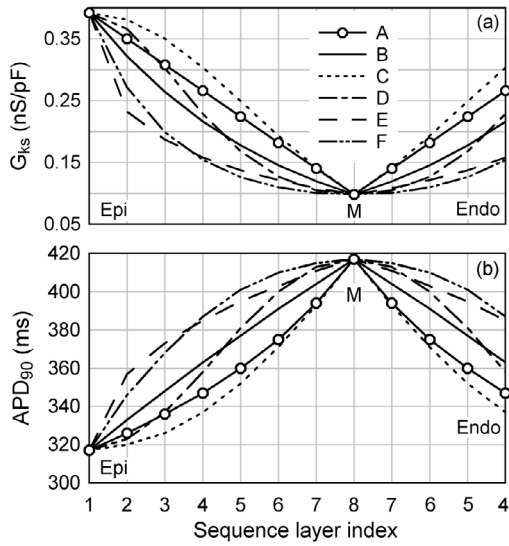


Figure 4. (a) distributions of maximal slow delayed rectifier current conductance ( $G_{Ks}$ ) and (b) resulting calculated distributions of action potential durations ( $APD_{90}$ ) for six distribution functions A-F described by Eqs. (15)-(21). The distributions correspond to the transverse cross-section of left lateral ventricular wall marked by black line in Figure 3.

### C. Distribution of Action Potential Duration

In our model we assume that ventricle APDs are distributed without significant discontinuities and boundaries between different ventricular cell types. To obtain such APD distribution in the ventricles taking into account M-cell concept, we set up our model to be in imaginary artificial condition in which simultaneous stimuli are applied at initial time instant 1 to the model cells on the outermost basal layer (basal epicardial surface). Then, the excitation front propagated in epicardial-to-endocardial and base-to-apex directions at a velocity so that at each step propagation proceeds one model cell ahead. Meanwhile, other stimuli are applied at time instants 2 and 4 to right and left ventricle basal endocardial surfaces, respectively, causing the propagation of excitation fronts in endocardial-to-epicardial

and base-to-apex directions with the same velocity. The excitation wave fronts meet in the depth of the midmyocardium and cancel each other. The time instants were chosen so as to yield the most realistic normal ECG waveforms.

The sequence number of excitation for a model cell corresponds to the particular APD value, thus the model cells with the same sequence number create layers with equal APD values. Midmyocardial zeniths appear in the points where the wave fronts come into contact. Figure 3 shows a horizontal cross-section of the heart model with APD distribution sequence thus obtained. The cell layers composing the islands with the maximal APD values are considered as M-cells.

The most important distinction between epicardial and M-cells APD is the difference in slow delayed rectifier current  $I_{Ks}$  value [1], and the APD is a function of maximal  $I_{Ks}$  conductance  $G_{Ks}$ . For calculation of AP waveform and  $APD_{90}$  value (determined as action potential duration at 90% repolarization) the dynamic restitution protocol proposed by Koller *et al* [26] was used. A series of 100 stimuli was generated at fixed cycle length (800 ms) until a steady-state APD is reached. This procedure was repeated to calculate  $APD_{90}$  for each cell layer number  $n$  ( $n = 1 \dots N$ ) changing the value of  $G_{Ks}$  from epicardial value  $G_{Ks}^{Epi}$  to midmyocardial value  $G_{Ks}^M$  with 6 different dependences on  $n$ :

$$(A): G_{Ks}^n = G_{Ks}^{Epi} - (n/N) \cdot (G_{Ks}^{Epi} - G_{Ks}^M) \quad (15)$$

- simple linear function and functions (B-F):

$$G_{Ks}^n = G_{Ks}^{Epi} \cdot \exp\left[\log\left(G_{Ks}^M / G_{Ks}^{Epi}\right) \cdot F_X\right], \quad (16)$$

where

$$F_B = n/N, \quad (17)$$

$$F_C = (n/N)^2, \quad (18)$$

$$F_D = [1 - \cos(\pi n/N)]/2, \quad (19)$$

$$F_E = \sqrt{n/N}, \quad (20)$$

and

$$F_F = 1 - (n/N)^2. \quad (21)$$

Here  $N = 8$  is maximal layer number (see Fig. 3).

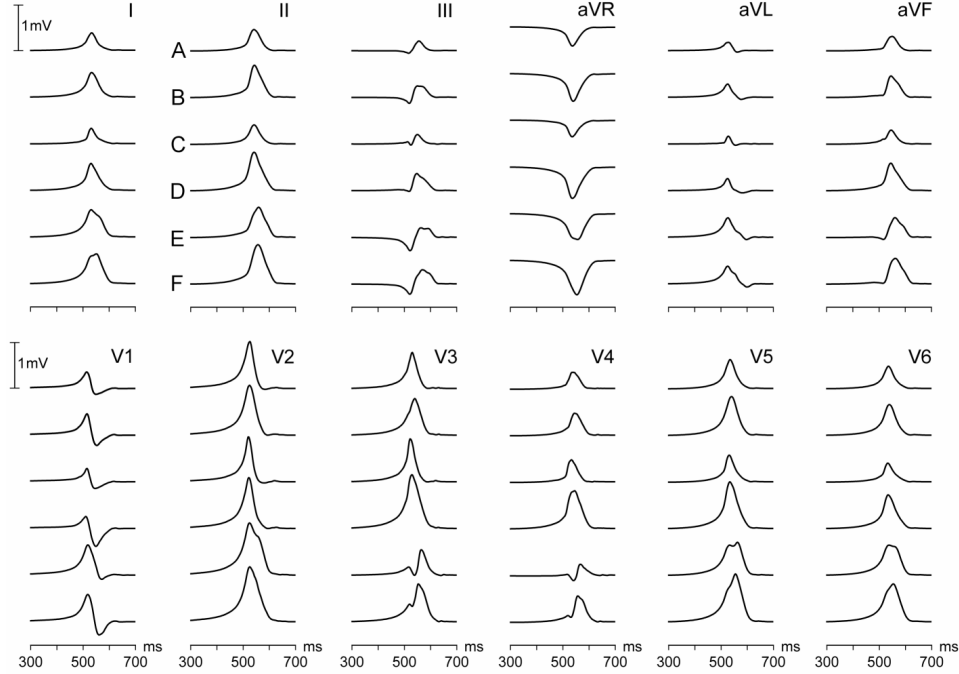


Figure 5. ECG waveforms with different T-wave shapes for six different  $APD_{90}$  distribution dependencies A-F described by Eqs. (15)-(21). P-wave and QRS complex are not shown. Horizontal axis shows time from beginning of the sinus rhythm.

#### D. T-wave Analysis

T-wave amplitude,  $Q-T_{peak}$  interval, and QT interval were measured on the obtained standard 12-lead ECG waveforms with the help of a simple MATLAB (The MathWorks, Natick, MA, USA) program. In the case of biphasic T-wave, its amplitude and apex position were determined by the highest absolute value of the amplitude. For the measurement of the QT interval, the Tangent method [27] was used to extrapolate the end of T-wave. We defined the latter as the intersection of the tangent to the steepest portion of the terminal limb of the T-wave with the isoelectric baseline.

### III. RESULTS

Figure 4 shows the  $G_{Ks}$  dependence on sequence layer index as well as resulting  $APD_{90}$  values distribution for the six dependences in question. Distribution of  $G_{Ks}$  value from midmyocardium to endocardium mirrorly repeats the epicardial-to-midmyocardial one. Then, we investigated the influence of proposed distributions of  $G_{Ks}$  value, and thus obtained distributions of  $APD_{90}$  values on the ECG waveforms, in particular, T-waves, performing single beat simulations with the cycle length of 800 ms.

Figure 5 demonstrates ECG waveforms with different T-wave shapes simulated for the  $APD_{90}$  distribution dependences calculated with the functions A-F [Eqs. (15)-(21)] shown in Fig. 4 and described in the previous section.

The obtained waveforms were analyzed in order to find out the most appropriate shape corresponding to the normal ECG ranges. For the distributions B, D, and F first limb of T-wave is moving faster then second limb which is abnormal for healthy human heart. The T-waves in case C are too weak and narrow. There are pronounced notches on T-waves in distribution E. Accordingly, for further simulation study we chose linear distribution of  $G_{Ks}$  [function A, Eq. (15)] since it yields more realistic T-wave shapes.

Figure 6 shows APD, excitation, and repolarization distributions for six different horizontal cross-sections of the model heart from base to apex calculated with the modified model. In the demonstrated APD distributions the cells with longest APD are located in the left ventricular wall and septum and the shortest one in right ventricle (Fig. 6a). The obtained APD gradients between apex and base and left and right ventricles are similar to reported in the experimental works [28-30]. The excitation sequence (Fig. 6b) resembles that described by Durrer *et al* in the human heart [31]. The repolarization time is shortest in the epicardial and endocardial cells, while it is longest in the midmyocardial cells (Fig. 6c) which follows from the summation of excitation sequence time and APD distribution.

Variation of the  $G_{Ks}$  value beyond the (ultimate) limits used in the original ion channel model [21] resulted in the significant deformation of the AP waveforms in AP phases 2 and 3. To change the dispersion of APD along with  $G_{Ks}$  value we used the variation of inactivation time constant  $\tau_f$

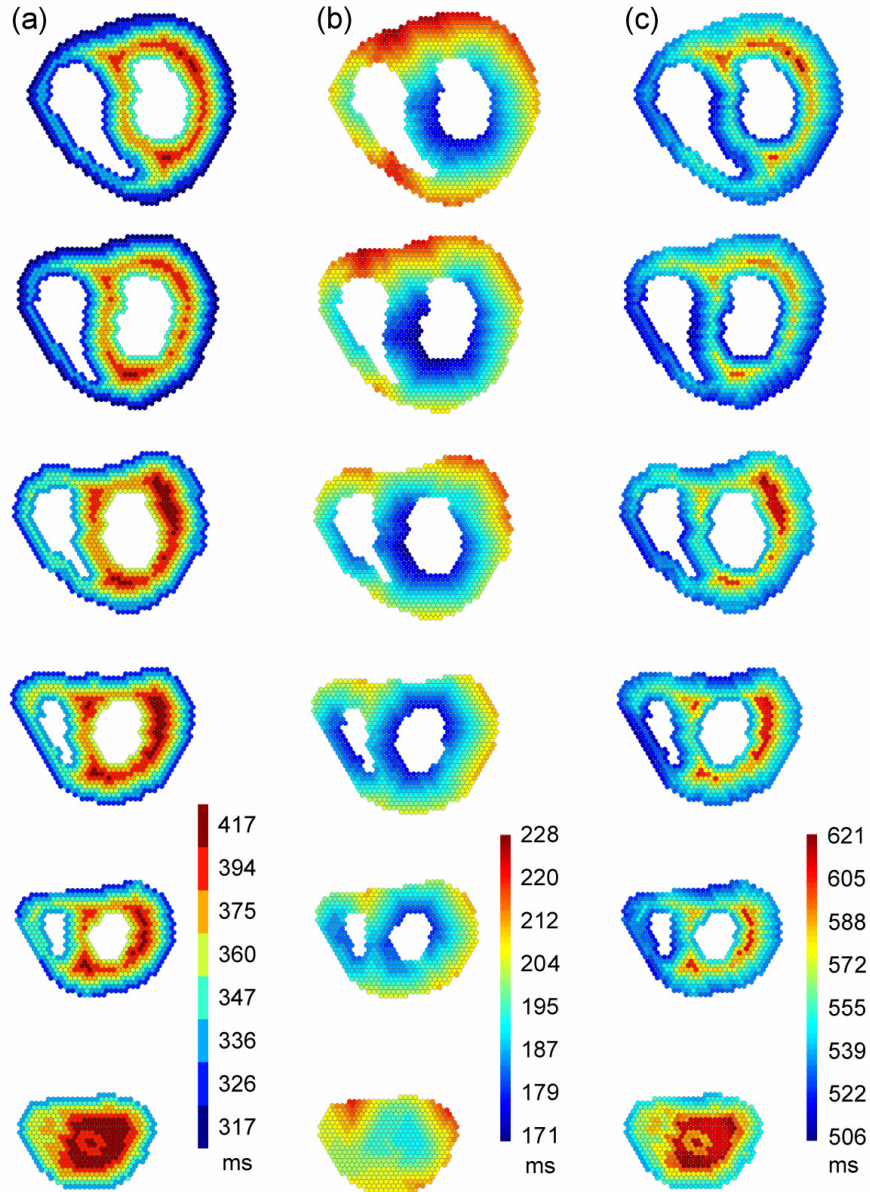


Figure 6. Action potential duration (a), excitation (b) and repolarization (c) distributions for six different horizontal cross-sections of model heart from base (top) to apex (bottom) for linear  $G_{Ks}$  distribution. The time for the excitation and repolarization is shown from beginning of the sinus rhythm.

for the  $f$  gate [21]. For this purpose, we introduced an additional parameter  $C\tau_f$  as a multiplication factor for  $\tau_f$ . The parameter  $C\tau_f$  was altered only for the voltage range  $V > 0$  mV, thus varying the inactivation but not recovery kinetics of L-type calcium current  $I_{CaL}$ . Resulting minimal and maximal  $APD_{90}$  values calculated with different  $C\tau_f$  are shown in Table 1.

Simulated ECG waveforms for lead V5 with variation of  $C\tau_f$  are demonstrated on the Fig. 7. The increase of  $C\tau_f$  (and, consequently, widening the positive voltage part of an AP) simultaneously for both minimal (epicardial) and maximal (midmyocardial) cells leads to rising of amplitude,

width, and end point of T-wave (see Fig. 7a). It is happened because of increasing contribution (the number) of myocardial cells with longer APD. The enlargement of  $C\tau_f$  for maximal and minimal  $APD_{90}$  separately leads to increasing transmural gradient of APD. In the Fig. 7b, longer maximal  $APD_{90}$  correlating with the repolarization of M-cells significantly prolongs QT interval, similar to reported in the works [32, 33]. Correspondently, the increase of minimal  $APD_{90}$  associated with prolongation of epicardial repolarization manifests in decreasing of ST segment duration (Fig. 7c).

Table 2. Minimal and maximal APD<sub>90</sub> values calculated with different  $C\tau_f$ .

$C\tau_f$	Minimal APD <sub>90</sub> , ms	Maximal APD <sub>90</sub> , ms
0.3		235
0.4	224	266
0.5	244	296
0.6	262	325
0.7	278	351
0.8	293	375
0.9	306	396
1.0	317	417
1.1	328	436
1.2	338	453
1.3	347	469
1.4	355	484
1.5	363	497
1.6	369	510

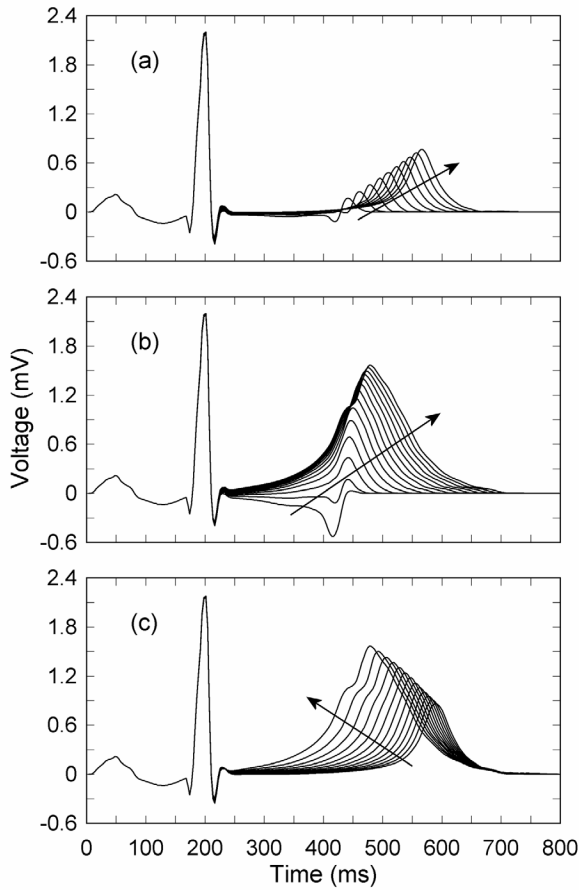


Figure 7. Calculated ECG waveforms (lead V5) for different values of  $C\tau_f$ : (a)  $C\tau_f$  increases from 0.4 to 1.3 along the arrow direction simultaneously for both minimal (epicardial) and maximal (midmyocardial) APD<sub>90</sub>; (b)  $C\tau_f$  is constant (0.4) for minimal APD<sub>90</sub> while it increases from 0.3 to 1.6 for maximal APD<sub>90</sub> along the arrow direction; (c)  $C\tau_f$  is constant (1.6) for maximal APD<sub>90</sub> while it increases from 0.4 to 1.6 for minimal APD<sub>90</sub> along the arrow direction.  $C\tau_f$  varies with 0.1 step for all figures here.

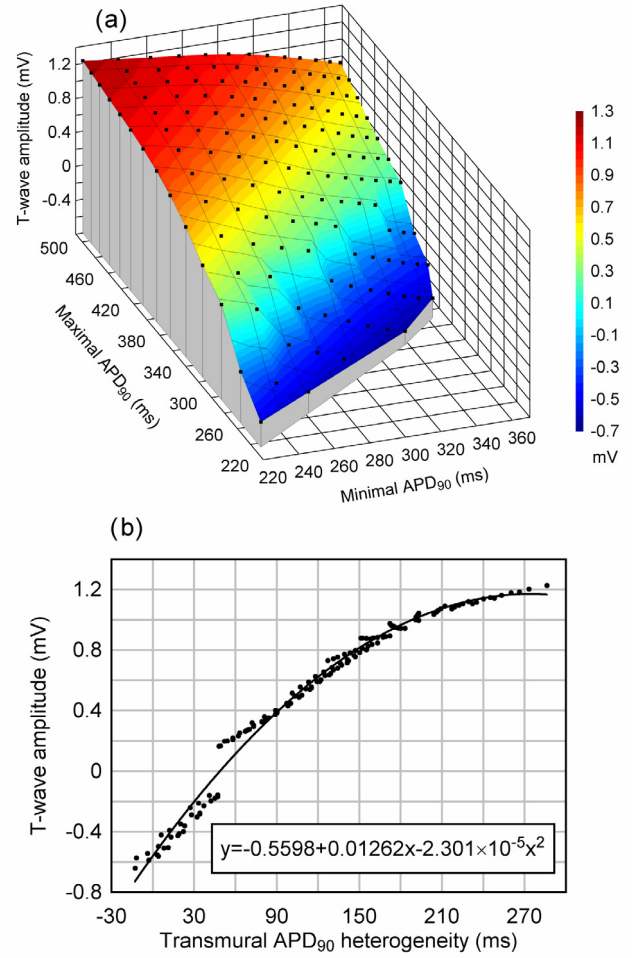


Figure 8. Dependence of T-wave amplitude (ECG lead II): (a) on minimal epicardial and maximal midmyocardial APD<sub>90</sub> values, (b) on transmural APD<sub>90</sub> heterogeneity. Black dots represent calculated ECG data points. Discontinuity in the data is caused by a transition between a monophasic and a biphasic T-wave.

Figure 8 shows relation between the T-wave amplitude and minimal epicardial and maximal midmyocardial APD<sub>90</sub> values for standard ECG lead II. General view of calculated data on T-wave amplitude in three dimensions is shown on Fig. 8a. The line on Fig. 8b is a polynomial fit (correlation coefficient is 0.99) of the calculated T-wave amplitude data plotted against the transmural heterogeneity, defined as the difference between maximal and minimal APD<sub>90</sub> values. The obtained dependence reveals slight nonlinear behavior with a tendency to saturation. At the transmural heterogeneity less than 60 ms the T-wave became negative.

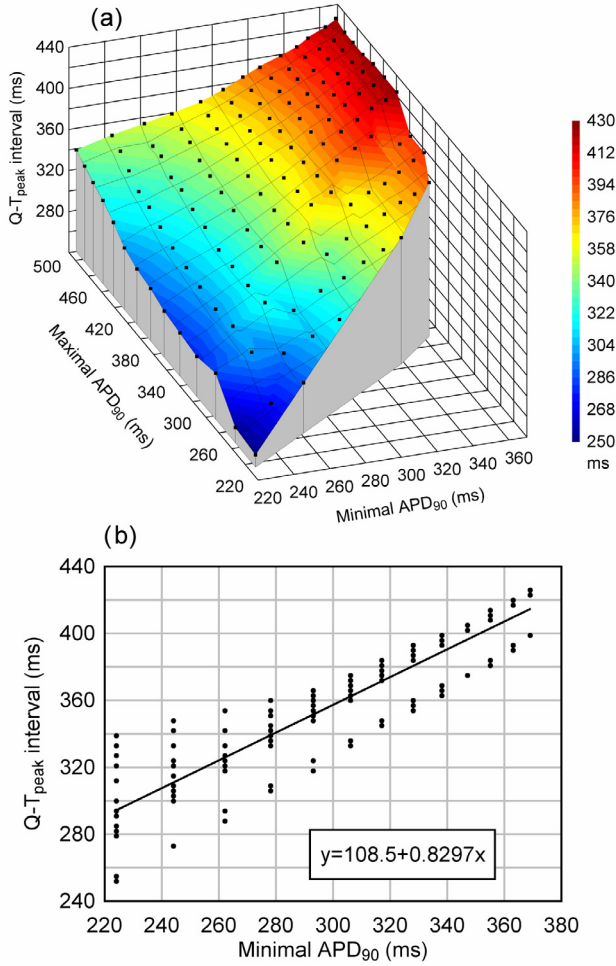


Figure 9. Dependence of Q-T<sub>peak</sub> interval (ECG lead II): (a) on minimal epicardial and maximal midmyocardial APD<sub>90</sub> values, (b) on minimal APD<sub>90</sub> value. Black dots represent calculated ECG data points.

Figure 9 depicts the dependence of Q-T<sub>peak</sub> interval on minimal and maximal APD<sub>90</sub> values in ECG lead II in three-dimensions and its linear polynomial fit against the minimal APD<sub>90</sub> with averaged maximal APD<sub>90</sub> value (correlation coefficient is 0.92).

QT interval dependence on minimal and maximal APD<sub>90</sub> values calculated for ECG lead II is demonstrated in Fig. 10. The three-dimensional graph on Fig. 10a shows weak dependence of QT interval magnitude on minimal APD<sub>90</sub> value. Despite big dispersion of the calculated data caused by the difficulty of the T-wave end detection, we extracted a polynomial fit (correlation coefficient is 0.83) of the second order plotted against maximal APD<sub>90</sub> value in Fig. 10b.

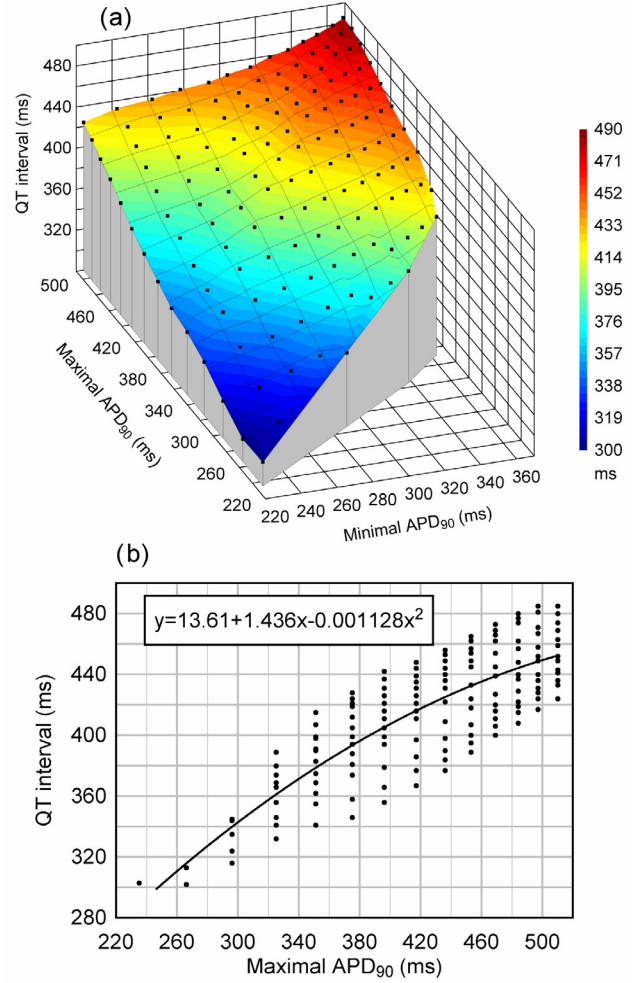


Figure 10. Dependence of QT interval (ECG lead II): (a) on minimal epicardial and maximal midmyocardial APD<sub>90</sub> values, (b) on maximal APD<sub>90</sub> value. Black dots represent calculated ECG data points.

#### IV. DISCUSSION

We demonstrated here new inhomogeneous continuous APD distribution utilizing 3D whole-heart model. Ventricular myocytes are heterogeneous due to regional variations in densities of membrane ionic currents. M-cells have the lowest density of  $I_{Ks}$  in the human ventricle [1] contributing to spatial dispersion of APDs.

We suppose that AP distribution is continuous in length from epicardium to midmyocardium, and from midmyocardium to endocardium. Thus, we assume that M-cells is conditional concept, they have longer APD than epicardial and endocardial cells, and have no specific morphological features. The study closest to our work was published by Trudel *et al* [12]. This researches obtained continuous APD distribution across the myocardium, with less APD deviation of three cell types in the thinner right ventricle.



Six different  $G_{Ks}$  distribution functions on layer index were considered. The linear  $G_{Ks}$  and corresponding APD dependences were chosen for further ECG simulations as demonstrating most realistic T-wave shapes.

The creation of T-wave depends on the difference between the shortest and the longest APs. We suppose that AP in epicardium is always shorter in comparison to endo- and midmyocardium. Midmural zeniths are located as islands of cells in the depth of thickest areas of ventricular tissue [34], which can reflect technical difficulties in finding and locating of M-cells experimentally. The controversy in M-cell existence is reflected in recent works [35, 36].

If the contraction rate is constant over the whole myocardium, the thick (left) ventricular wall shrinks and relaxes slower than the thin (right) wall, thus cells in thick wall should have longer APD, and so the range of M-cells region could be a functional behavior [37].

Amplitude and wideness of T-wave increase with enlarging the difference between minimal (epicardial) and maximal (midmyocardial) APD values. The decreasing of transmural heterogeneity leads to diminishing of T-wave parameters and its absence results in negative T-wave in most ECG leads, which is not physiological. Our results support the existence of M-cells as well as transmural heterogeneity in healthy human heart. However, the M-cell definition in our case seems to be inexplicit because the maximal APD values are different in different parts of myocardium, for right and left ventricles, the base and apex, even for one horizontal cross-section of the heart.

Using our proposed transmural distribution of APD we obtained natural ratios of the T-wave amplitudes in different ECG leads (Fig. 5): in lead I the T-wave is higher than in lead III, in lead VI it is lower than in lead V6, and it is negative in lead aVR.

The transmural repolarization gradient is caused by the voltage difference of minimal and maximal APDs. To increase the heterogeneity we prolonged maximal and shortened minimal myocardial potentials which went beyond the physiological limits of normal heart function, thus mimicking pathological conditions such as short and long QT syndromes. In the case of homogeneous and weak heterogeneous myocardium we obtained negative T-waves, while increase of the transmural gradient resulted in the enlargement of the T-wave amplitude and width (Fig. 8). The polarity of the T-wave can be changed in a controlled manner [35].

The  $Q-T_{peak}$  interval reflects final repolarization of epicardial cells, consequently with increase of minimal APD value the epicardial cells repolarize later [32, 33]. In our simulations we obtained almost linear dependence  $Q-T_{peak}$  on minimal APD value while no significant relation between maximal APD and  $Q-T_{peak}$  were observed (Fig. 9).

The QT interval is known to be related to final repolarization of the midmyocardial cells. These cells have the longest APD and thus repolarize last. So the end of the

T-wave depends on the length of maximal APD, which is demonstrated by the results of our simulations (Fig. 10).

## V. LIMITATIONS

In the present work we employed simplified approach for the modulation of APD using only variation of maximal slow delayed rectifier current conductance  $G_{Ks}$  and time constant for  $f$  gate  $C\tau_f$ . We only focused on the study of influence of the AP length on the T-wave morphology, since the role of the AP shape is insignificant for the normal heart. Thus we did not include into our ion channel model any differences between midmyocardial and endocardial cells in values of transient outward current  $I_{to}$ , which is responsible for the distinction between AP shapes in phase 1. Also, if new experimental data on other ionic currents underlying AP waveform variation throughout myocardial tissue become available, the utilization of these currents may improve our model.

Although the whole heart model used in this study is rather simple and computationally efficient, the increase of current model cells spatial resolution of 1.5 mm may improve precise tuning of M-cells location in the midmyocardium and fine spatial APD distribution, which is especially important for the simulation of the arrhythmias.

## VI. CONCLUSIONS

We proposed the computer model which includes combination of ion channel cellular AP model and 3D whole heart structure with continuous and inhomogeneous APD distributions which is a function of  $G_{Ks}$  distribution. The APD distribution depends on the thickness of the myocardium, with the longest APDs located in the left ventricle and septum. The obtained results demonstrated that transmural heterogeneity is essential to T-wave formation and are in a good agreement with experimental observations [32, 35], in particular, T-wave amplitude closely correlates with transmural  $APD_{90}$  heterogeneity, maximal AP duration approximates QT interval, and  $Q-T_{peak}$  linearly depends on minimal AP duration.

Our simulations demonstrated the validity of the proposed continuous heterogeneous APD distribution with islands (zeniths) of M-cells [34]. The proposed original APD distribution is reasonable and produces realistic ECG waveforms.

## VII. APPENDIX. MODIFICATION OF ION CHANNEL MODEL

The cell membrane is modeled as a capacitor connected in parallel with variable resistances and batteries representing the different ionic currents and pumps. The electrophysiological behavior of a single cell is described using Hodgkin-Huxley-type formalism [38]:

Table 2. Model parameters for our modified ion channel model.

Parameter	Definition	Value
$G_{NaL}$	Maximal $I_{NaL}$ conductance	0.0113 nS/pF
$\tau_{hL}$	Inactivation time constant for $I_{NaL}$	600 ms
$v_{max}$	Maximal flux of $I_{NaCa}$	8.8 pA/pF
$k_{NaCa}$	Maximal $I_{NaCa}$	1.000 pA/pF
$\gamma$	Voltage dependence parameter of $I_{NaCa}$	0.35
$K_{mCaDis}$	Intracellular Ca dissociation constant for $I_{NaCa}$	0.0036 mmol/L
$K_{mNaDis}$	Intracellular Na dissociation constant for $I_{NaCa}$	12.3 mmol/L
$K_{mCaAct}$	Half-maximal Ca induced activation of $I_{NaCa}$	$1.50 \times 10^{-4}$ mmol/L
$k_{sat}$	Saturation factor for $I_{NaCa}$ at negative potentials	0.27

$$\frac{\partial V}{\partial t} = -\frac{I_{ion} + I_{stim}}{C_m}, \quad (A1)$$

where  $V$  is the transmembrane potential,  $t$  is time,  $I_{stim}$  is the externally applied stimulus current,  $C_m$  is the cell capacitance per unit surface area, and  $I_{ion}$  is the sum of all transmembrane ionic currents:

$$I_{ion} = I_{Na} + I_{KI} + I_{Io} + I_{Kr} + I_{Ks} + I_{CaL} + I_{NaCa} + I_{NaK} + I_{pCa} + I_{pK} + I_{bCa} + I_{bNa} + I_{NaL}. \quad (A2)$$

$$\Delta E = \frac{v_{max} \left[ Na_i^3 Ca_o \exp(\gamma VF/RT) - Na_o^3 Ca_i \exp((\gamma-1)VF/RT) \right]}{\left[ 1 + k_{sat} \exp((\gamma-1)VF/RT) \right] \left[ \frac{K_{mCa} Na_i^3 + K_{mNa}^3 Ca_i + K_{mNaDis}^3 Ca_o (1 + Ca_i/K_{mCaDis})}{+ K_{mCaDis} Na_o^3 (1 + Na_i^3/K_{mNaDis}^3) + Na_i^3 Ca_o + Na_o^3 Ca_i} \right]}. \quad (A5)$$

Here  $F$  is Faraday's constant,  $R$  is the universal gas constant,  $T = 310$  K is temperature,  $Ca_i$  and  $Na_i$ ,  $Ca_o$  and  $Na_o$  are intracellular and extracellular ionic concentrations of calcium and sodium, respectively,  $K_{mCa}$  and  $K_{mNa}$  are half-saturation constants for  $I_{NaCa}$ , respectively.

For activation of  $I_{NaL}$  we use kinetics and steady-state voltage dependence of  $I_{NaL}$  from original ten Tusscher and Panfilov model [21]:

$$I_{NaL} = G_{NaL} m_L^3 h_L (V - E_{NaL}), \quad (A6)$$

where  $m_L$  and  $h_L$  are activation and inactivation gates for  $I_{NaL}$ , respectively. The voltage dependence and kinetics of inactivation are based on data from human ventricular myocytes [43, 44] (see Table 2 for parameters). The formulation of  $I_{NaL}$  inactivation was adapted from Hund and Rudy [41]. Equilibrium late  $Na^+$  potential  $E_{NaL}$  was calculated in accordance with the Nernst equation:

$$E_{NaL} = \frac{RT}{F} \ln \left( \frac{Na_o}{Na_i} \right). \quad (A7)$$

Here  $I_{Na}$  is fast sodium current,  $I_{KI}$  is inward rectifier potassium current,  $I_{Io}$  is transient outward current,  $I_{Kr}$  and  $I_{Ks}$  are rapid and slow delayed rectifier potassium currents, respectively,  $I_{CaL}$  is L-type calcium current,  $I_{NaCa}$  is sodium-calcium exchanger current,  $I_{NaK}$  is sodium-potassium pump current,  $I_{pCa}$  is sarcolemmal calcium pump current,  $I_{pK}$  is plateau potassium current,  $I_{bCa}$  and  $I_{bNa}$  are background calcium and sodium currents, respectively, and  $I_{NaL}$  is late (slowly inactivating) sodium current.

The original formulation of  $I_{NaCa}$  was based on the guinea pig model [39]. In this study we used the allosteric formulation of  $I_{NaCa}$  introduced by Weber *et al* [40] where  $I_{NaCa}$  was represented by an electrochemical ( $\Delta E$ ) and an allosteric ( $Allo$ ) factors. This formulation was included in canine cardiac ventricular cell model of Hund and Rudy [41] with parameters for canine myocyte.

We accepted the data from the work of Weber *et al* [42] for human ventricular cells and did not use any additional factor enhancing outward nature of  $I_{NaCa}$  (see Table 2 for parameters):

$$I_{NaCa} = Allo \cdot \Delta E, \quad (A3)$$

where

$$Allo = \frac{1}{1 + (K_{mCaAct}/Ca_i)^2}, \quad (A4)$$

The equations for the activation and inactivation gates are as follows:

$$m_L^i = m_\infty + (m_L^{i-1} - m_\infty) \exp(-\Delta t / \tau_m); \quad (A8)$$

$$m_\infty = \frac{1}{\left( 1 + \exp\left( \frac{-56.86 - V}{9.03} \right) \right)^2}; \quad (A9)$$

$$\tau_m = \frac{1}{1 + \exp\left( \frac{-60 - V}{5} \right)} \times \left\{ \frac{0.1}{1 + \exp\left( \frac{V + 35}{5} \right)} + \frac{0.1}{1 + \exp\left( \frac{V - 50}{200} \right)} \right\}; \quad (A10)$$

$$h_L^i = h_{L\infty} + (h_L^{i-1} - h_{L\infty}) \exp(-\Delta t / \tau_{hL}); \quad (\text{A11})$$

$$h_{L\infty} = \frac{1}{1 + \exp\left(\frac{V + 94}{6.9}\right)}; \quad (\text{A12})$$

where  $\Delta t$  is time step,  $\tau_m$  and  $\tau_{hL}$  are activation and inactivation time constants for  $I_{NaL}$ , respectively, and  $i$  is the iteration index. Equations (A8) and (A11) represent the solution of gating equations [38] with Rush-Larsen method [45].

Regional differences in  $I_{NaL}$  have been described for canine [46] and guinea pig myocardium [47], with guinea pig M-cells having a smaller  $I_{NaL}$  and canine M-cells having a larger  $I_{NaL}$  than the other cell types, and differences in the density of  $I_{NaCa}$  have been described for canine myocardium [48], with M-cells having a larger exchanger current. Because of the contradictory and insufficient experimental data for human myocytes, we did not include these differences in the description of transmural heterogeneity of our model.

## REFERENCES

- [1] D.-W. Liu and C. Antzelevitch, "Characteristics of the delayed rectifier current ( $I_{Kr}$  and  $I_{Ks}$ ) in canine ventricular epicardial, midmyocardial, and endocardial myocytes," *Circ. Res.*, vol. 76, pp. 351-365, 1995.
- [2] E. P. Anyuhovsky, E. A. Sosunov, and M. R. Rosen, "Regional differences in electrophysiological properties of epicardium, midmyocardium, and endocardium. In vitro and in vivo correlations," *Circulation*, vol. 94, pp. 1981-1988, 1996.
- [3] C. Antzelevitch, "Heterogeneity of cellular repolarization in LQTS: the role of M cells," *Eur. Heart J.*, vol. 3 suppl. K, pp. K2-K16, 2001.
- [4] E. Drouin, F. Charpentier, C. Gauthier, K. Laurent, and H. Le Marec, "Electrophysiological characteristics of cells spanning the left ventricular wall of human heart: evidence for presence of M cells," *J. Am. Coll. Cardiol.*, vol. 26, pp. 185-192, 1995.
- [5] G.-R. Li, J. Feng, L. Yue, and M. Carrier, "Transmural heterogeneity of action potentials and  $I_{to1}$  in myocytes isolated from the human right ventricle," *Am. J. Physiol. Heart Circ. Physiol.*, vol. 275, pp. 369-377, 1998.
- [6] P. Colli Franzone, L. F. Pavarino, S. Scacchi, and B. Taccardi, "Monophasic action potentials generated by bidomain modeling as a tool for detecting cardiac repolarization times," *Am. J. Physiol. Heart Circ. Physiol.*, vol. 293, pp. H2771-H2785, 2007.
- [7] J. V. Tranquillo, D. O. Burwell, and C. S. Henriquez, "Analytical model of extracellular potentials in a tissue slab with a finite bath," *IEEE Trans. Biomed. Eng.*, vol. 52 (2), pp. 334-338, 2005.
- [8] G.-X. Yan, W. Shimizu, and C. Antzelevitch, "The controversial M cell," *Circulation*, vol. 98, pp. 1921-1927, 1998.
- [9] E.P. Anyuhovsky, E.A. Sosunov, R. Z. Gainullin, and M.R. Rosen, "Regional differences in electrophysiological properties of epicardium, midmyocardium, and endocardium. In vitro and in vivo correlations," *Circulation*, vol. 94, pp. 1981-1988, 1996.
- [10] N. Trayanova, "Defibrillation of the heart: insights into mechanisms from modelling studies," *Exp. Physiol.*, vol. 91(2), pp. 323-337, 2006.
- [11] K. J. Sampson and C. G. S. Henriquez, "Simulation and prediction of functional block in the presence of structural and ionic heterogeneity," *Am. J. Physiol. Heart Circ. Physiol.*, vol. 281, pp. H2597-H2603, 2001.
- [12] M.-C. Trudel, B. Dubé, M. Potse, R. M. Gulrajani, and L. J. Leon, "Simulation of QRST integral maps with a membrane-based computer heart model employing parallel processing," *IEEE Trans. Biomed. Eng.*, vol. 51, pp. 1319-1329, 2004.
- [13] M. Aoki, Y. Okamoto, T. Musha, and K. Harumi, "Three-dimensional simulation of the ventricular depolarization and repolarization processes and body surface potentials: normal heart and bundle branch block," *IEEE Trans. Biomed. Eng.*, vol. BME-34(6), pp. 454-462, 1987.
- [14] K. Harumi, M. J. Burgess, and J. A. Abildskov, "A theoretic model of the T wave," *Circulation*, vol. 34, pp. 657-668, 1966.
- [15] D. Wei, G. Yamada, T. Musha, H. Tsunakawa, T. Tsutsumi, and K. Harumi, "Computer simulation of supraventricular tachycardia with the Wolff-Parkinson-White syndrome using three-dimensional heart models," *J. Electrocardiol.*, vol. 23 (3), pp. 261-173, 1990.
- [16] D. Wei, O. Okazaki, K. Harumi, E. Harasawa, and H. Hosaka, "Comparative simulation of excitation and body surface electrocardiogram with isotropic and anisotropic computer heart models," *IEEE Trans. Biomed. Eng.*, vol. 42(4), pp. 343-357, 1995.
- [17] D. Wei, "Whole-heart modeling: progress, principles and applications," *Prog. Biophys. molec. Biolol.*, vol. 67(1), pp. 17-66, 1997.
- [18] D. Wei, "Whole heart modeling and simulation," *Modeling and Imaging of Bioelectrical Activity: Principles and Applications*, (ed. B. He), pp. 81-117, Norwell (MA): Kluwer Academic, 2004.
- [19] X. Zhu and D. Wei, "Computer simulation of intracardiac potential with whole-heart model," *Int. J. Bioinformatics Research and Applications*, vol. 3(1), pp. 100-122, 2007.
- [20] E. Ryzhii and D. Wei, "Computer simulation of atypical Brugada syndrome," *J. Electrocardiol.*, vol. 42, pp. 319-327, 2009.
- [21] K. H. W. J. ten Tusscher and A.V. Panfilov, "Alternans and spiral breakup in a human ventricular tissue model," *Am. J. Physiol. Heart Circ. Physiol.*, vol. 291, pp. H1088-H1100, 2006.
- [22] G. Li, C. Lau, T. Leung, and S. Nattel, "Ionic current abnormalities associated with prolonged action potentials in cardiomyocytes from diseased human right ventricles," *Heart Rhythm*, vol. 4, pp. 460-468, 2004.
- [23] R. F. Gilmour, J. J. Heger, E. N. Prystowsky, and D. Z. Zipes, "Cellular electrophysiologic abnormalities of diseased human ventricular myocardium," *Am. J. Cardiol.*, vol. 51, pp. 137-144, 1983.
- [24] C. A. Brebbia, "The boundary element method for engineers," London, Pentech Press, 1980.
- [25] W. T. Miller and D. B. Geselowitz, "Simulation studies of the electrocardiogram. I. The normal heart," *Circ. Res.*, vol. 43, pp. 301-315, 1978.
- [26] M. L. Koller, M.L. Riccio, and R. F. Gilmour, "Dynamic restitution of action potential duration during electrical alternans and ventricular fibrillation," *Am. J. Physiol. Heart Circ. Physiol.*, vol. 275, pp. H1635-H1642, 1998.
- [27] E. Lepschkin and B. Surawicz, "The measurement of the QT interval of the electrocardiogram," *Circulation*, vol. 6, pp. 378-88, 1952.
- [28] M. J. Janse, E. A. Sosunov, R. Coronel, T. Opthof, E. P. Anyukhovskiy, J. M. T. De Bakker, A. N. Plotnikov, I. N. Shlapakova, P. Danilo, J. G. P. Tijssen, and M. R. Rosen, "Repolarization gradients in the canine left ventricle before and after induction of short-term cardiac memory," *Circulation*, vol. 112, pp. 1711-1718, 2005.
- [29] Y. Xia, Y. Liang, O. Kongstad, Q. Liao, M. Holm, B. Olsson, and S. Yuan, "In vivo validation of the coincidence of the peak and end of the T wave with the full repolarization of the epicardium and endocardium in swine," *Heart Rhythm*, vol. 2, pp. 162-169, 2005.
- [30] P. G. A. Volders, K. Sipido, E. Carmeliet, R. L. Spatjens, H. J. Wellens, and M. A. Vos, "Repolarizing  $K^+$  currents  $I_{to}$  and  $I_{Ks}$  are larger in right than in left canine ventricular myocardium," *Circulation*, vol. 99, pp. 206-210, 1999.
- [31] D. Durrer, R. T. Van Dam, G. E. Freud, M. J. Janse, F. L. Meijler, and R. C. Arzbaecher, "Total excitation of the isolated human heart," *Circulation*, vol. 41, pp. 899-912, 1970.
- [32] C. Antzelevitch, "Heterogeneity and cardiac arrhythmias: An overview," *Heart Rhythm*, vol. 4(7), pp. 964-972, 2007.
- [33] C. Antzelevitch, "Role of spatial dispersion of repolarization in inherited and acquired sudden cardiac death syndromes," *Am. J. Physiol. Heart Circ. Physiol.*, vol. 293, pp. H2024-H2038, 2007.

- [34] F. G. Akar, G. X. Yan, C. Antzelevitch, and D. S. Rosenbaum, "Unique topographical distribution of M cells underlies reentrant mechanism of torsade de pointes in the long-QT syndrome," *Circulation*, vol. 105, pp. 1247–53, 2002.
- [35] C. Patel, J. F. Burke, H. Patel, P. Gupta, P. R. Kowey, C. Antzelevitch, and G.-X. Yan, "Is there a significant transmural gradient in repolarization time in the intact heart. Cellular basis of the T wave," *Circ. Arrhythmia Electrophysiol.*, vol. 2, pp. 80–88, 2009.
- [36] T. Opthof, R. Coronel, and M. J. Janse, "Is there a significant transmural gradient in repolarization time in the intact heart. Repolarization gradients in intact heart," *Circ. Arrhythmia Electrophysiol.*, vol. 2, pp. 89–96, 2009.
- [37] N. Ueda, D. P. Zipes, and J. Wu, "Functional and transmural modulation of M cell behavior in canine ventricular wall," *Am. J. Physiol. Heart Circ. Physiol.*, vol. 287, pp. H2569–H2575, 2004.
- [38] A. L. Hodgkin and A. F. Huxley, "A quantitative description of membrane current and its application to conduction and excitation in nerve," *J. Physiol.*, vol. 117, pp. 500–544, 1952.
- [39] D. Noble, A. Varghese, P. Kohl, and P. Noble, "Improved guinea-pig ventricular cell model incorporating a diadic space,  $I_{Kr}$  and  $I_{Ks}$ , and length and tension-dependent processes," *Can. J. Cardiol.*, vol. 14, pp. 123–134, 1998.
- [40] C. R. Weber, K. S. Ginsburg, K. D. Philipson, T. R. Shannon, and D. M. Bers, "Allosteric regulation of  $\text{Na}^+ - \text{Ca}^{2+}$  exchange current by cytosolic Ca in intact cardiac myocytes," *J. Gen. Physiol.*, vol. 117, pp. 119–131, 2001.
- [41] T. J. Hund and Y. Rudy, "Rate dependence and regulation of action potential and calcium transient in a canine cardiac ventricular cell model," *Circulation*, vol. 110, pp. 3168–3174, 2004.
- [42] C. R. Weber, V. Piacentino, S. R. Houser, and D. M. Bers, "Dynamic regulation of sodium/calcium exchange function in human heart failure," *Circulation*, vol. 108, pp. 2224–2229, 2003.
- [43] V. A. Maltsev, H. N. Sabbah, R. S. D. Higgins, N. Silverman, M. Lesch, and A. I. Undrovinas, "Novel, ultraslow inactivating sodium current in human ventricular myocytes," *Circulation*, vol. 98, pp. 2545–2552, 1998.
- [44] V. A. Maltsev, H. N. Sabbah, and A. I. Undrovinas, "Late sodium current is a novel target for amiodarone: studies in failing human myocardium," *J. Mol. Cell. Cardiol.*, vol. 33, pp. 923–932, 2001.
- [45] S. Rush and H. Larsen, "A practical algorithm for solving dynamic membrane equations," *IEEE Trans. Biomed. Eng.*, vol. 25(4), pp. 389–392, 1978.
- [46] A. C. Zygmunt, G. T. Eddlestone, G. P. Thomas, V. V. Nesterenko, and C. Antzelevitch, "Larger late sodium conductance in M cells contributes to electrical heterogeneity in canine ventricle," *Am. J. Physiol. Heart Circ. Physiol.*, vol. 281, pp. H689–H697, 2001.
- [47] B. F. A. S. Sakmann, A. J. Spindler, S. M. Bryant, K. W. Linz, and D. Noble, "Distribution of a persistent sodium current across the ventricular wall in guinea pig," *Circ. Res.*, vol. 87, pp. 910–914, 2000.
- [48] A. C. Zygmunt, R. J. Goodrow, and C. Antzelevitch, " $I_{\text{NaCa}}$  contributes to electrical heterogeneity within the canine ventricle," *Am. J. Physiol. Heart Circ. Physiol.*, vol. 278, pp. H1671–H1678, 2000.